Optical activity and birefringence of the incommensurate phase of Rb_2ZnCl_4

J. Kobayashi
Kagami Memorial Laboratory for Material Science and Technology, Waseda University, 2-8-26 Nishi-Waseda, Shinjuku-ku, Tokyo 169, Japan
and Research Development Corporation of Japan, 2-5-2 Nagata-cho, Chiyoda-ku, Tokyo 100, Japan

K. Saito, N. Takahashi, I. Kamiya, and H. Utsumi
Kagami Memorial Laboratory for Material Science and Technology, Waseda University, 2-8-26 Nishi-Waseda, Shinjuku-ku, Tokyo 169, Japan
(Received 25 March 1994)

By using the high-accuracy universal polarimeter, all the components of optical activity tensor g and birefringence Δn of Rb_2ZnCl_4, which were studied in limited part before, have been reexamined. A unique component, g_{23}, was definitely found to appear both in the incommensurate and ferroelectric phases, but all the other components vanished in the two phases. The previous report is revised. It manifests a similar temperature dependence to that found in $[N(CH_3)_4]_2ZnCl_4$; it changes the sign within the temperature region of the incommensurate phase. This phenomenon can be interpreted as due to the difference of optical gyration of soliton regions and that of the commensurate domains. It was confirmed that the critical exponent, approximately 0.42, of the temperature dependence of g_{23} agrees with nearly constant values shown by other various A_2BX_4 crystals. However, temperature, where the multisoliton region emerges, was found to differ considerably from that of $[N(CH_3)_4]_2ZnCl_4$.

I. INTRODUCTION

Measurements of optical activity (OA) of the crystals became possible by the invention of high-accuracy universal polarimeter (HAUP).[1] As a result, interesting new phenomena concerning physical properties and phase transitions of crystals have been revealed. One of the important findings brought about by HAUP was the OA of the incommensurate (IC) phases of A_2BX_4-type crystals. This was discovered by Kobayashi, *et al.*[2] in $(NH_4)_2BeF_4$. Subsequent to this crystal, various crystals belonging to this group were reported to be optically active, e.g., K_2SeO_4,[3] Rb_2ZnCl_4 (RZC),[4] $[N(CH_3)_4]_2ZnCl_4$ (TMAZC),[5] and $[N(CH_3)_4]_2CuCl_4$ (TMACC),[6] etc. However, as the OA were generally 10^{-3} order of magnitude less than birefringences, the accuracy of HAUP in the early stage was not sufficient for measuring accurately the OA of these crystals. A conspicuous advantage of the HAUP method was to remove exhaustively systematic errors, which had been overlooked for ordinary polarimetric measurements, but should be critical for measurements of OA. Three years after the invention of HAUP, Kobayashi, Kumoni, and Saito[7] found a systematic error $\delta\Upsilon$, which took place in setting up a crossed Nicol system. Correction of $\delta\Upsilon$ increased conspicuously the accuracy of the HAUP measurements, and since then, the major systematic errors were removed from the HAUP method, in principle.

In spite of such a progress in the principles of the HAUP method, the real measurements were not sufficiently satisfactory. The existence of OA in the IC phases was not convincing. Dijkstra, Kremers, and Meekes[8] performed first comprehensive HAUP measurements of OA and birefringence of TMAZC using six specimens with different orientations. They found that all the components g_{ij}—except for g_{11}—existed not only in the IC phase, but also in the paraelectric phase. Ortega *et al.*[9] studied the OA of the IC phase of Rb_2ZnBr_4 (RZB) in two different orientations and TMACC in one orientation using the HAUP method and reached the conclusion that the IC phases of these crystals lacked OA.

Kobayashi *et al.*[10,11] recently made comprehensive measurements of OA and birefringences of TMAZC and RZB using specimens of the six different orientations and clarified the fact that a unique gyration component g_{23} undoubtedly took place in each IC phase. Thus these studies on the two crystals have stimulated the necessity of extending comprehensive measurements of HAUP to a wider variety of crystals for extracting accurate information of OA existing in the IC phases of the A_2BX_4 group.

Kobayashi *et al.*[4] reported the temperature dependence of g_{23} of RZC. However, our recent reexaminations on the previous result by using the advanced HAUP indicated that it was not perfectly correct and needs revisions by the comprehensive measurements. This paper reports the results of the study.

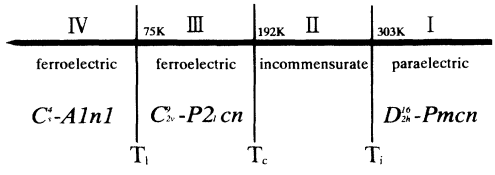

FIG. 1. Schematic representation of the phase diagram of Rb_2ZnCl_4.

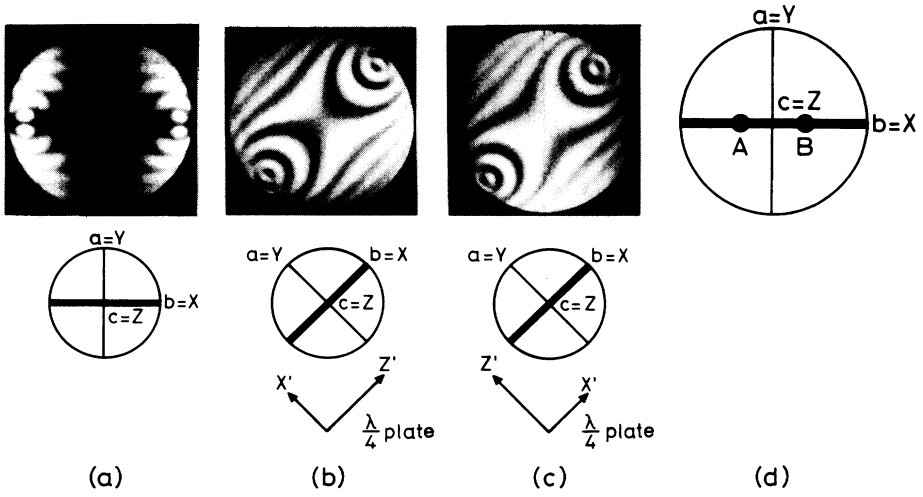

FIG. 2. Optical nature of Rb_2ZnCl_4 at room temperature (a) Conoscopic figure in the extinction position; (b), (c) conoscopic figures in the diagonal subtracting and adding conditions respectively produced by the insertion of the quarter-wavelength plates; and (d) stereographic representation of the optical nature.

II. HAUP EXPERIMENTS

A. Specimens

The phase diagram of RZC is shown schematically in Fig. 1, the transition temperatures separating the phases I, II, III, and IV being defined T_i, T_c, and T_l as indicated in the figure. Phase I in the paraelectric state is centrosymmetrical, the space group being orthorhombic D_{2h}^{16} with lattice constant $a=7.28$ Å, $b=12.73$ Å, and $c=9.26$ Å.[12] An incommensurate modulation of the superlattice in phase II takes place along the c axis,[13] and the commensurate superlattice is recovered in phase III with a period of $3c$. The spontaneous polarization P_s appears along the a axis in phase III,[14] whose space group is C_{2v}^9. Phase IV is also ferroelectric and belongs to a monoclinic space group C_s^4, where P_s is contained in the (010) plane.[15] The principal axes x_1, x_2, and x_3 of the

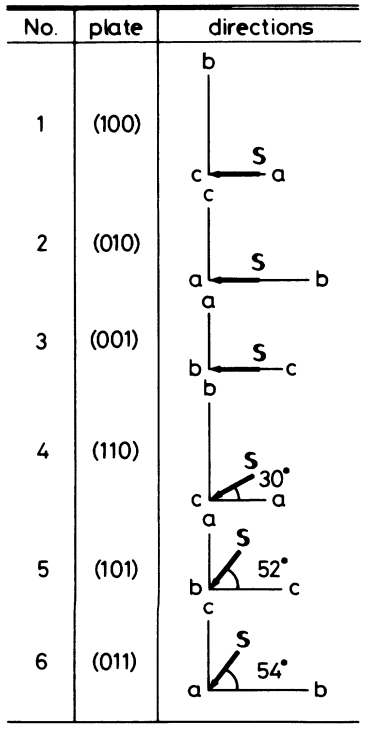

FIG. 3. Directions of the wave vector s of the incident light with respect to the crystallographic axes of the six specimens.

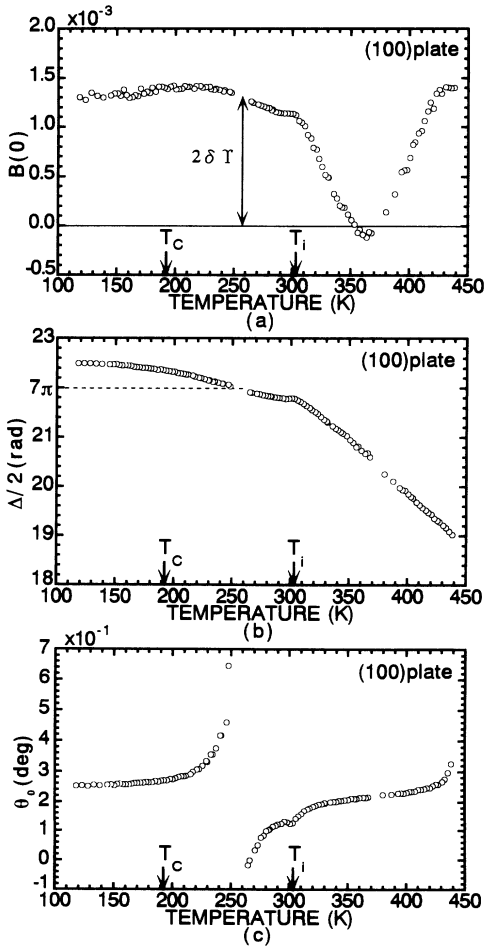

FIG. 4. Temperature dependences of (a) $B(0)$, (b) $\Delta/2$, and (c) θ_0, of the (100) specimen of Rb_2ZnCl_4.

dielectric impermeability tensor are taken along the crystallographic a, b, and c axes of phase I in what follows.

The crystals were grown by cooling an aqueous solution of RbCl and $ZnCl_2$ in 2:1 molar ratio from 304.0 to 299.2 K with a cooling rate of -0.24 K/day. The crystals were colorless.

The optical nature of RZC was determined at room temperature by using a polarizing microscope. A conoscopic figure of a (001) plate specimen in extinction position is shown in Fig. 2(a), where it is clearly shown that two optic axes are contained in the (100) plane. This means that the a axis corresponds optically to the Y axis. When quarter-wavelength plates were inserted, the conoscopic figures in diagonal positions were changed as seen in Figs. 2(b) and 2(c), where different optical orientations of the quarter-wavelength plates are indicated; Fig. 2(b) indicated a subtracting figure between the plate and the specimen, while Fig. 2(c) indicated an adding figure. In this way, we determined the optical orientation of RZC as depicted in Fig. 2(d).

We prepared six specimens numbered 1–6 with surface planes of the following indices: (100), (010), (001), (110), (101), and (011). Surfaces of each specimen were polished by alumina powder with a homogeneous grain size of 0.2 μm.

When light was incident perpendicular to the (100),

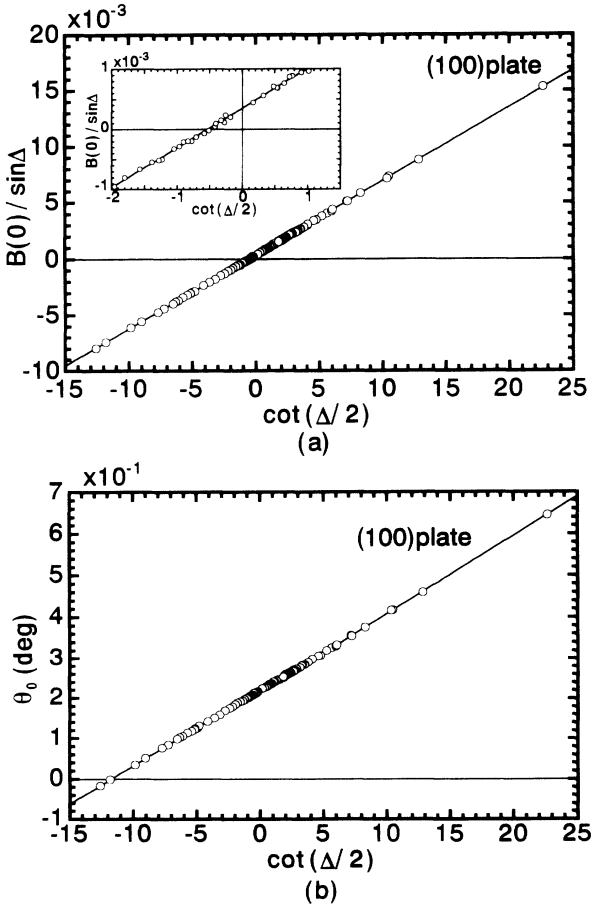

FIG. 5. Relations of (a) $B(0)/\sin\Delta$ and (b) θ_0 with respect to $\cot(\Delta/2)$ for the (100) specimen of Rb_2ZnCl_4.

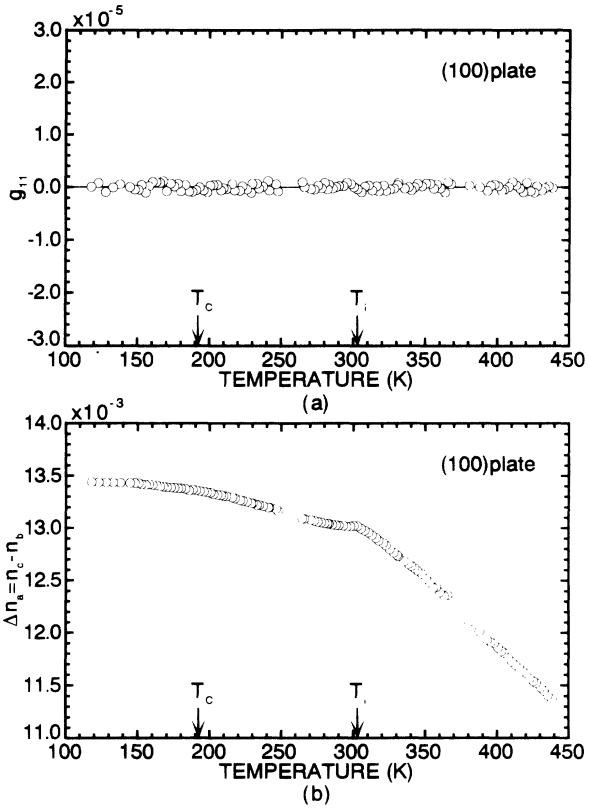

FIG. 6. Temperature dependences of (a) g_{11} and (b) Δn_a of Rb_2ZnCl_4.

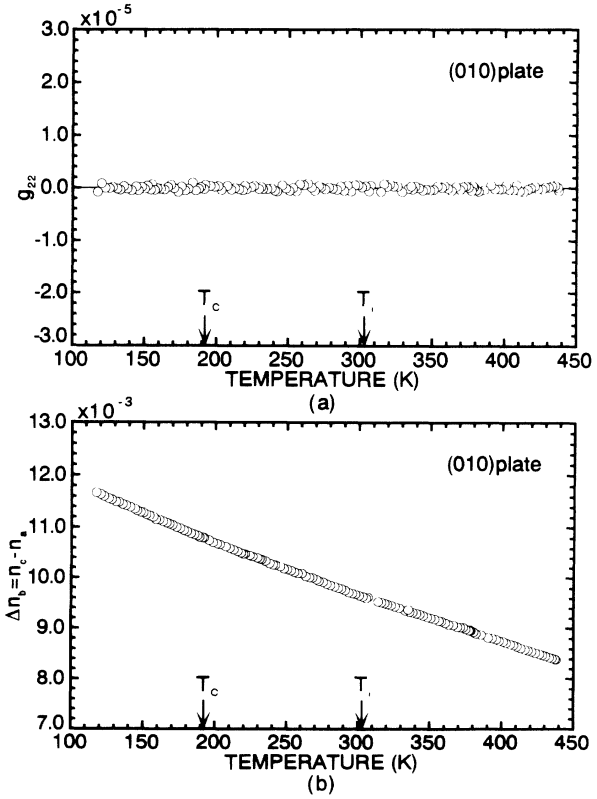

FIG. 7. Temperature dependences of (a) g_{22} and (b) Δn_b of Rb_2ZnCl_4.

TABLE I. Data for specimens used in the present experiment.

Sample no.	Surface planes	Birefringence Δn	Gyration G	Area (mm^2)	Thickness (mm)
1	(100)	$\Delta n_a = n_c - n_b$	$G_a = g_{11}$	2.2×3.3	0.260
2	(010)	$\Delta n_b = n_c - n_a$	$G_b = g_{22}$	2.4×2.7	0.153
3	(001)	$\Delta n_c = n_a - n_b$	$G_c = g_{33}$	1.8×2.3	0.148
4	(110)	$\Delta n_{(110)} = 0.75\Delta n_a + 0.25\Delta n_b$	$G_{(110)} = 0.75g_{11} + 0.25g_{22} + 0.87g_{12}$	2.6×3.5	0.284
5	(101)	$\Delta n_{(101)} = 0.62\Delta n_a + 0.38\Delta n_c$	$G_{(101)} = 0.62g_{11} + 0.38g_{33} + 0.97g_{13}$	3.0×3.8	0.369
6	(011)	$\Delta n_{(011)} = 0.35\Delta n_b - 0.65\Delta n_c$	$G_{(011)} = 0.35g_{22} + 0.65g_{33} + 0.95g_{23}$	2.0×3.2	0.198

(010), and (001) surface specimens, the following birefringences and gyrations could be measured: $\Delta n_{(100)} \equiv \Delta n_a = n_c - n_b$, $\Delta n_{(010)} \equiv \Delta n_b = n_c - n_a$, $\Delta n_{(001)} \equiv \Delta n_c = n_a - n_b$, and $G_{(100)} = g_{11}$, $G_{(010)} = g_{22}$, and $G_{(001)} = g_{33}$. For the (110), (101), and (011) specimens, the observed birefringences $\Delta n_{(110)}$, $\Delta n_{(101)}$, and $\Delta n_{(011)}$ could be expressed in terms of Δn_a, Δn_b, and Δn_c after some computation described in detail in Ref. 10. In Fig. 3, the relations between the wave vector s of the incident light and the crystallographic axes are shown for the six samples. In Table I, the surface planes, birefringence, gyration, area, and thickness of each specimen are tabulated.

B. Measurements

HAUP measurements were made on the samples placed in a vacuum chamber and held at various temperatures within an accuracy of ±0.02 K. The light source was an Ar laser with a wavelength of 4880 Å. $B(0)$, retardation Δ, and characteristic angles θ_0 were measured at various temperatures. These quantities are related by

$$B(0) = (\gamma - 2k)\sin\Delta + 2\delta\Upsilon\cos^2(\Delta/2)\ , \tag{1}$$

or equivalently

$$B(0)/\sin\Delta = \gamma - 2k + \delta\Upsilon\cot(\Delta/2) \tag{2}$$

and

$$\theta_0 = -\tfrac{1}{2}(p+q)\cot(\Delta/2) - \tfrac{1}{2}\delta\Upsilon + \Psi\ . \tag{3}$$

Here k represents the ellipticity of the elliptically polarized wave traveling in the specimen, and Ψ is the rotation angle of the indicatrix. γ and $\delta\Upsilon$ are the principal systematic errors; p and q designate the parasitic ellipticities of the polarizer and analyzer, respectively, and $\delta\Upsilon$ is the deflected angle from the accurate crossed Nicols condition as mentioned in Ref. 7.

The measurements were performed at first on the (100)

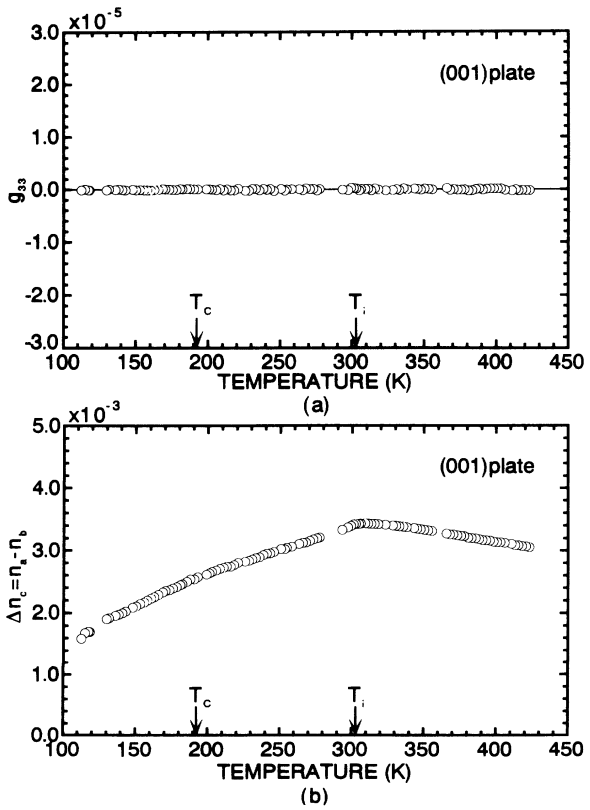

FIG. 8. Temperature dependences of (a) g_{33} and (b) Δn_c of Rb_2ZnCl_4.

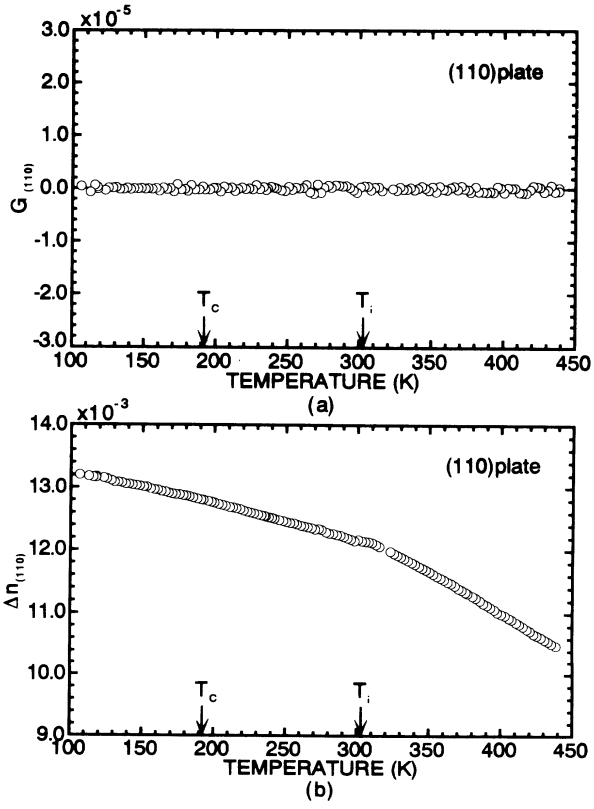

FIG. 9. Temperature dependences of (a) $G_{(110)}$ and (b) $\Delta n_{(110)}$ of Rb_2ZnCl_4.

TABLE II. Systematic errors in the six optical systems.

Sample no.	p ($\times 10^{-4}$)	q ($\times 10^{-4}$)	γ ($\times 10^{-4}$)	$\delta\Upsilon$ ($\times 10^{-4}$)
1	−1.52	−5.04	3.52	6.59
2	−2.40	2.95	−5.35	2.37
3	−4.48	−2.13	−2.35	−7.68
4	1.20	3.93	−2.73	10.80
5	−2.49	−4.05	1.56	4.93
6	−1.50	−2.91	1.41	3.69

surface specimen in the temperature range from 438 down to 118 K. The temperature dependences of $B(0)$, $\Delta/2$, and θ_0 are depicted in Figs. 4(a), 4(b), and 4(c), respectively. θ_0 manifested typical divergences at 259 K, where $\Delta/2$ became 7π. $B(0)/\sin\Delta$ and θ_0 are plotted with respect to $\cot(\Delta/2)$ in Figs. 5(a) and 5(b), respectively. It is clearly seen that $B(0)/\sin\Delta$ showed a strict linear change. This indicated that γ, $\delta\Upsilon$, and k were kept constant in the whole temperature range. The linear variation of θ_0 also shows the constancy of Ψ as well as p, q, and $\delta\Upsilon$. It is certain from the symmetry of phase I that k and Ψ are zero in phase I. Therefore it was concluded that $k=0$ from Fig. 5(a) and $\Psi=0$ from Fig. 5(b) in the whole temperature range. γ and $\delta\Upsilon$ were determined as 3.52×10^{-4} and 6.59×10^{-4} form an enlarged version in the inset of Fig. 5(a). We can calculate g_{11} and

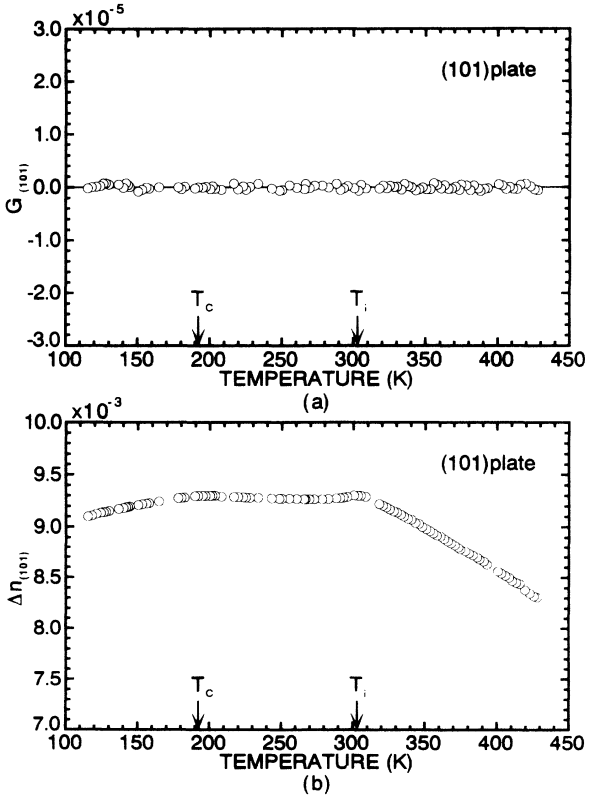

FIG. 10. Temperature dependences of (a) $G_{(101)}$ and (b) $\Delta n_{(101)}$ of Rb_2ZnCl_4.

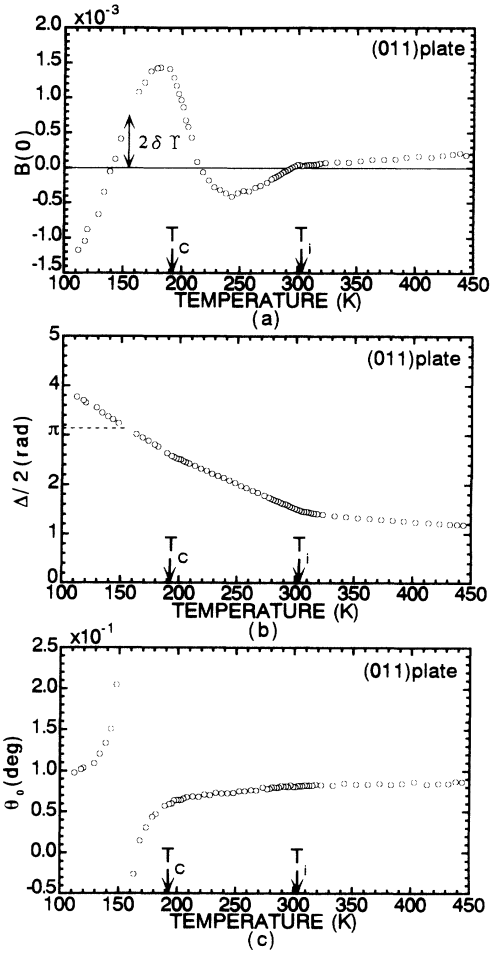

FIG. 11. Temperature dependences of (a) $B(0)$, (b) $\Delta/2$, and (c) θ_0, of the (011) specimen of Rb_2ZnCl_4.

Δn_a by using these error parameters. The results are depicted in Figs. 6(a) and 6(b) as a function of temperature. g_{11} was found to be zero in the whole temperature range, and Δn_a showed a sudden change in the slope at T_i, but did not at T_c.

Similar measurements were performed on samples Nos. 2–5. Detailed descriptions are omitted here, but strict

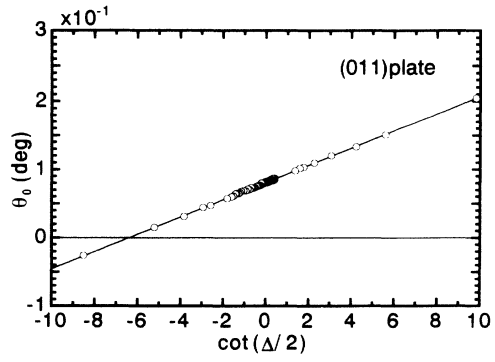

FIG. 12. Plot of θ_0 with respect to $\cot(\Delta/2)$ for the (011) specimen of Rb_2ZnCl_4.

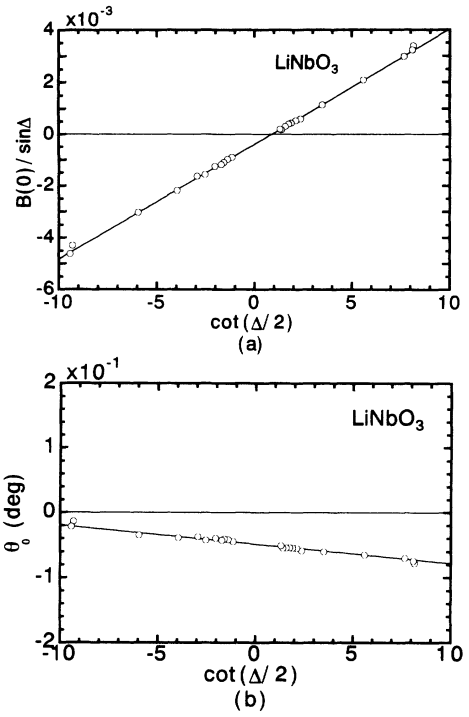

FIG. 13. Plots of (a) $B(0)/\sin\Delta$ and (b) θ_0 with respect to $\cot(\Delta/2)$ for the (100) surface specimen of $LiNbO_3$.

linear relations of $B(0)/\sin\Delta$ and θ_0 were observed against $\cot(\Delta/2)$ for these samples. The systematic errors obtained from these relations are tabulated in Table II. The temperature dependences of gyration and birefringence of samples 2–5 are represented in Figs. 7–10. In any orientations of RZC shown in these figures, gyrations did not take place at all in the mentioned temperature range. The birefringence manifested sudden changes in slopes at T_i in the (001), (110), and (101) specimens.

The temperature dependences of $B(0)$, $\Delta/2$, and θ_0 are depicted in Figs. 11(a), 11(b), and 11(c) for the (011) specimen with area of 2.0×3.2 mm^2 and thickness of 0.198 mm. The change of $\Delta/2$ in phase I of this specimen was found to be small. Then we paid attention to the fact

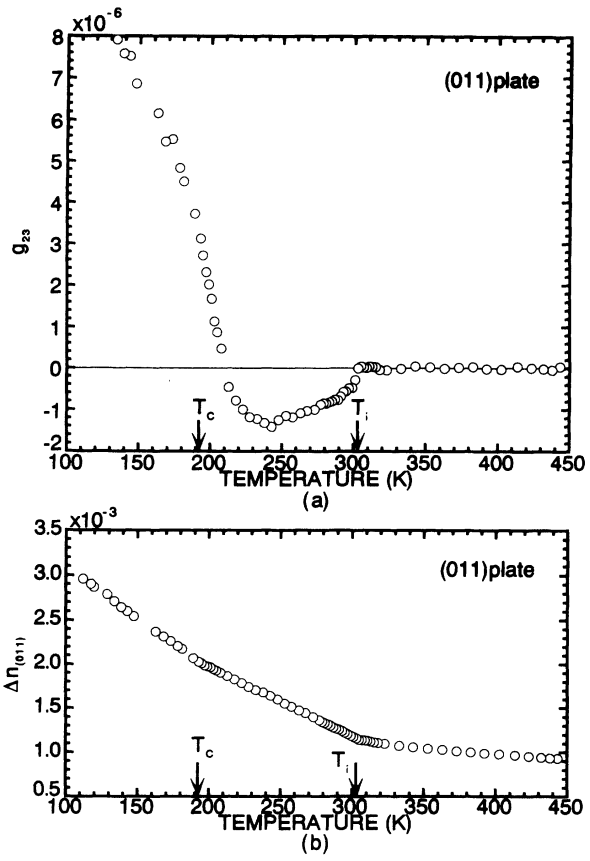

FIG. 15. Temperature dependences of (a) g_{23} and (b) $\Delta n_{(011)}$ of Rb_2ZnCl_4.

that the results obtained by using (2) might be inaccurate, and adopted the method (2) mentioned in Ref. 10 for evaluating the systematic errors. A specimen with a thickness producing a retardation of $2n\pi$ (n is an integer) at some temperature was intentionally prepared for obtaining $\delta\Upsilon$. Another error parameter γ was estimated by using a standard crystal of $LiNbO_3$.[16] $\Delta/2$ of the present specimen became π at 152 K, and consequently θ_0 manifested divergences at this temperature. $\delta\Upsilon$ was immediately determined to be 3.69×10^{-4} from $B(0)$. The

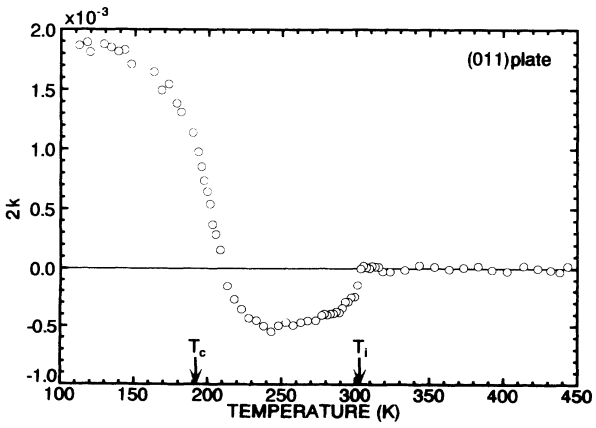

FIG. 14. Temperature dependence of $2k$ of Rb_2ZnCl_4.

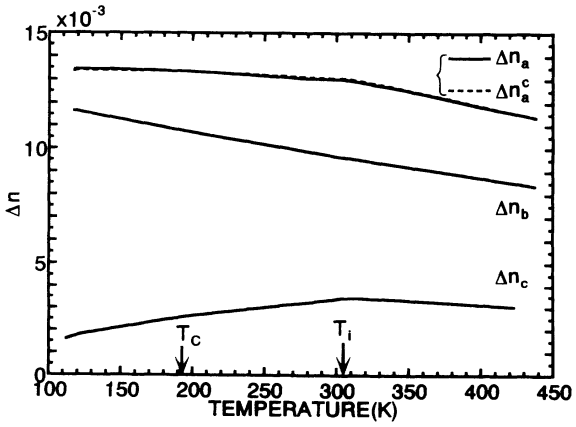

FIG. 16. Temperature dependences of Δn_a, Δn_b, and Δn_c of Rb_2ZnCl_4.

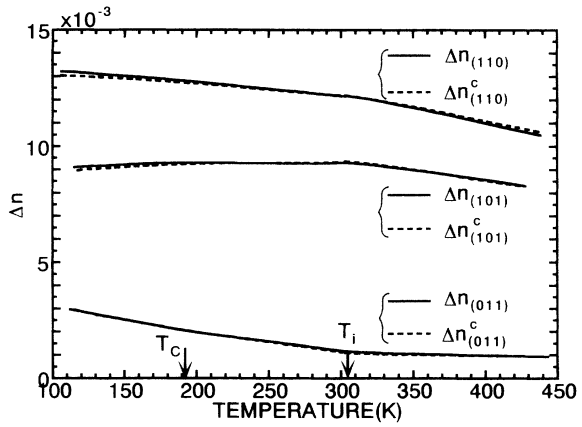

FIG. 17. Temperature dependences of $\Delta n_{(110)}$, $\Delta n_{(101)}$, and $\Delta n_{(011)}$ of Rb_2ZnCl_4.

change of θ_0 with respect to $\cot(\Delta/2)$ is represented in Fig. 12. A strict linear relation held between them. Then it was found that $\hat{p}+q$ was -4.41×10^{-4} and $\Psi=0$, where $\hat{p}$ represents the systematic error p which was common to this and $LiNbO_3$ systems.

Subsequently, the same measurements as in the (011) specimen were made on a (100) plate of $LiNbO_3$ with an area of 2.6×3.9 mm^2 and a thickness of 0.262 mm. The plots of $B(0)/\sin\Delta$ and θ_0 against $\cot(\Delta/2)$ are shown in Figs. 13(a) and 13(b). From Fig. 13(a) the error parameter $\gamma'=\hat{p}-q'$ was evaluated as -4.01×10^{-4}, and from Fig. 13(b), $\hat{p}+q'$ as 1.01×10^{-4}. From both values, $\hat{p}$ could be determined as -1.50×10^{-4}. By using this value, q of the (011) specimen was obtained as -2.91×10^{-4}, and finally γ was evaluated to be 1.41×10^{-4}. By using these values of $\delta\Upsilon$ and γ, the temperature dependence of $2k$ was derived as shown in Fig. 14. It is clearly seen that it becomes nonzero below T_i. $g_{23}(=G_{(011)}/0.95)$ and $\Delta n_{(011)}$, thus derived, are shown in Figs. 15(a) and 15(b), respectively. g_{23} appears at T_i,

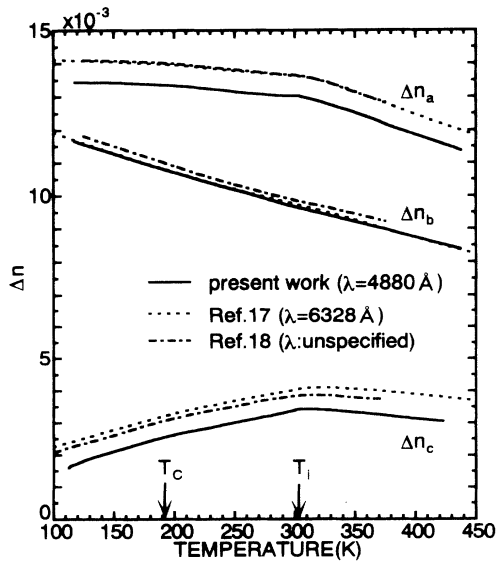

FIG. 18. Comparison of Δn_a, Δn_b, and Δn_c of Rb_2ZnCl_4 with those obtained by other workers.

but changes its sign at 18 K above T_c.

Birefringences along the principal directions, Δn_a, Δn_b, and Δn_c, are depicted in Fig. 16, and those along the diagonal directions, $\Delta n_{(110)}$, $\Delta n_{(101)}$, and $\Delta n_{(011)}$, in Fig. 17. The calculated birefringence $\Delta n_a^c=\Delta n_b+\Delta n_c$, shown by the dashed line in Fig. 16, coincides completely with Δn_a. The calculated birefringence $\Delta n^c_{(110)}$, etc., in terms of Δn_a, Δn_b, and Δn_c, is also shown in Fig. 17 by the dashed lines. The agreement of the observed and calculated birefringences is also excellent here, proving the sufficient accuracy of the present HAUP measurements. A comparison of birefringences Δn_a, Δn_b, and Δn_c with those reported by Günter, Sanctuary, and Rohner[17] and Kroupa and Fousek[18] is made in Fig. 18. Agreements of the results of the three groups are generally good. However, the measurements by Mel'nikova and Anistratov,[19] not shown in the figure, do not agree with the present results.

III. DISCUSSION

It has been revealed that a unique component g_{23} appears in the IC and ferroelectric phases of RZC, but the other five components do not. The temperature dependence of g_{23} of RZC is similar to that of the same component of TMAZC, which was shown in Fig. 7(a) in Ref. 10; it increases once from T_i, reverses the sign, and increases again with decrease of temperature. Below T_c, it continues to increase monotonically. Here the fact that both crystals manifest opposite signs in g_{23} indicates that the class of IC phases of both crystals can be regarded nearly as C_{2v}, where g_{23} measured from (011) and (01$\bar{1}$) planes should be opposite in the signs.

We have already interpreted in Ref. 7 the reason of such behavior of a gyration component displayed by TMAZC. Therefore RZC belongs to the same, 3_1-type, as TMAZC classified there. As has already been explained by Kobayashi,[20] and Saito and Kobayashi,[21] the origin of OA of IC phases can be ascribed to the occurrence of the helical phason mode. Then the observed gyration values g^{ob} should be proportional to the magnitude of the amplitude mode, viz., the radius of the helical mode, which modulates existing periods incommensurately. The temperature dependence of g^{ob} can be expected to be

$$|g^{ob}|=|g_p|=\alpha(T_i-T)^{\beta}\ . \tag{4}$$

$|g^{ob}|$ values are plotted with respect to (T_i-T) on logarithmic scales in Fig. 19. It is seen from the figure that

TABLE III. Critical exponents of A_2BX_4 crystals.

Substance	Critical exponent	Reference
Rb_2ZnCl_4	0.42	Present work
Rb_2ZnBr_4	0.40	11
$[N(CH_3)_4]_2ZnCl_4$	0.42	10
$[N(CH_3)_4]_2CuCl_4$	0.43	6
$(C_3H_7NH_3)_2MnCl_4$		
Higher-temperature region	0.44	21
Lower-temperature region	0.42	21

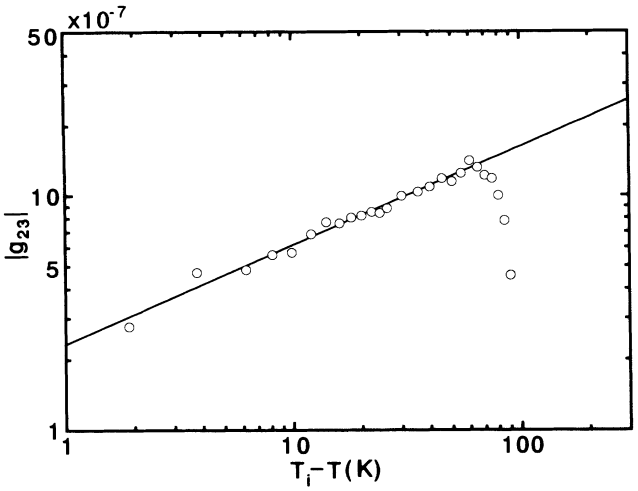

FIG. 19. Plots of g_{23} of Rb_2ZnCl_4 with respect to $(Ti-T)$ on a logarithmic scale.

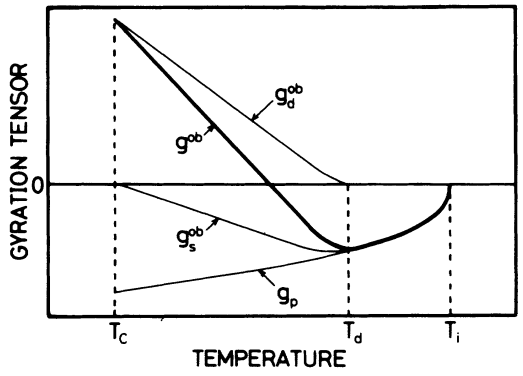

FIG. 20. Schematic representation of the temperature dependences of g^{ob}, g_p, g_s^{ob}, and g_d^{ob} for 3_1-type crystals.

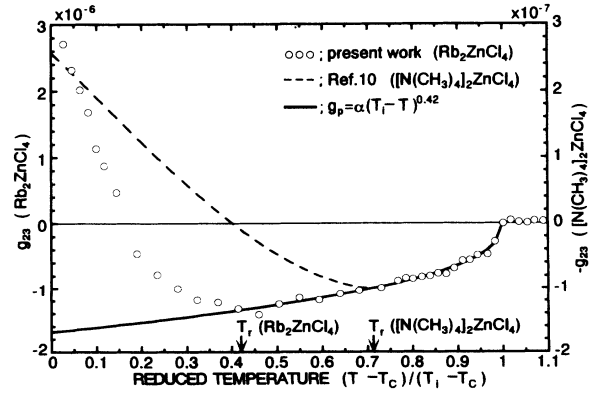

FIG. 21. Comparison of the temperature dependences of g_{23} of Rb_2ZnCl_4 and $[N(CH_3)_4]_2ZnCl_4$.

TABLE IV. T_r of A_2BX_4 crystals.

Substance	T_r	Reference
Rb_2ZnCl_4	0.42	Present work
Rb_2ZnBr_4	0.63	11
$[N(CH_3)_4]_2ZnCl_4$	0.72	10
$[N(CH_3)_4]_2CuCl_4$	0.35	6

(4) holds strictly by the critical exponent $\beta=0.42$ with $\alpha=2.3\times10^{-7}$. It is of interest that this critical exponent lies within the nearly constant values ~0.40–0.44, common to other A_2BX_4 crystals as seen in Table III. This fact confirms the validity of our interpretation of the origin of OA of IC phases.

As the temperature decreases, the helical structure begins to collapse, and the crystal is segregated into solitons and commensurate domains regions. In this region g^{ob} is the sum of gyrations of the segregated two regions.

$$g^{ob}=g_s^{ob}+g_d^{ob}\ , \tag{5}$$

where g_s^{ob} represents observed gyration of the solitons region, while g_d^{ob} domains region. Each term can be expressed as

$$g_s^{ob}=n_s g_p \tag{6}$$

and

$$g_d^{ob}=\sum_j (1-n_s) r|Ps_j|\ . \tag{7}$$

Here n_s designates soliton density, Ps_j, spontaneous polarization of the jth domain, and r an electrogyration coefficient. Then the temperature dependence of a gyration tensor of the 3_1-type crystal ($g_s^{ob}\cdot g_d^{ob}<0$) is schematically depicted in Fig. 20. Here there should exist a temperature T_d, where the segregation begins to take place. It is 239 K in RZC.

In order to compare the temperature dependences of g_{23} of RZC and TMAZC, they are expressed with respect to the reduced temperature $(T-T_c)/(T_i-T_c)$ in Fig. 21. As has been mentioned above, the behaviors in the phason region are completely coincided. However, a characteristic reduced temperature $T_r=(T_d-T_c)/(T_i-T_c)$, when the multisoliton region emerges, differs considerably between the two crystals. In fact, T_r as tabulated in Table IV, scatters among various other crystals. Elucidation of the behavior of n_s in the multisolitons region is another significant problem for understanding the lock-in transition to the commensurate phase. Nevertheless, in the present cases of RZC And TMAZC, knowledge of spontaneous polarizations appearing in the commensurate domains is indispensable for this discussion. This needs some theoretical treatment. We will study the lock-in transition mechanism after more and accurate experimental data of related crystals are accumulated.

ACKNOWLEDGMENT

This work was supported by the Research Development Corporation of Japan.

[1]J. Kobayashi and Y. Uesu, J. Appl. Crystallogr. **16**, 204 (1983).
[2]J. Kobayashi, Y. Uesu, J. Ogawa, and Y. Nishihara, Phys. Rev. B **31**, 4569 (1985).
[3]Y. Uesu and J. Kobayashi, Ferroelectrics **64**, 115 (1985).
[4]J. Kobayashi, K. Saito, H. Fukase, and K. Matsuda, Phase Trans. **15**, 225 (1988).
[5]J. Kobayashi and K. Saito, Proc. Jpn. Acad. **62**, 177 (1986).
[6]K. Saito, H. Sugiya, and J. Kobayashi, J. Appl. Phys. **68**, 732 (1990).
[7]J. Kobayashi, H. Kumomi, and K. Saito, J. Appl. Crystallogr. **19**, 377 (1986).
[8]E. Dijkstra, M. Kremers, and H. Meekes, J. Phys. Condens. Matter **4**, 715 (1992).
[9]J. Ortega, J. Etxebarria, J. Zubillaga, T. Breczewski, and M. J. Tello, Phys. Rev. B **45**, 5155 (1992).
[10]J. Kobayashi, K. Saito, N. Takahashi, and I. Kamiya, Phys. Rev. B **48**, 10038 (1993).
[11]J. Kobayashi, K. Saito, N. Takahashi, and I. Kamiya, Phys. Rev. B **49**, 6539 (1994).
[12]M. Harada, Ann. Rep. Res. Reactor Inst. Kyoto Univ. **14**, 51 (1981).
[13]K. Gesi and M. Iizumi, J. Phys. Soc. Jpn. Lett. **46**, 697 (1979).
[14]S. Sawada, Y. Shiroishi, A. Yamamoto, M. Takashige, and M. Matsuo, J. Phys. Soc. Jpn. Lett. **43**, 2099 (1977).
[15]H.-G. Unruh and J. Strömich, Solid State Commun. **39**, 737 (1981).
[16]J. Kobayashi, T. Asahi, S. Takahashi, and A. M. Glazer, J. Appl. Crystallogr. **21**, 479 (1988).
[17]P. Günter, R. Sanctuary, and F. Rohner, Phys. Status Solidi A **70**, 583 (1982).
[18]J. Kroupa and J. Fousek, Jpn. J. Appl. Phys. **24**, 784 (1985).
[19]S. V. Mel'nikova and A. T. Anistratov, Fiz. Tverd. Tela (Leningrad) **25**, 848 (1983) [Sov. Phys. Solid State **25**, 485 (1983)].
[20]J. Kobayashi, Phys. Rev. B **42**, 8332 (1990).
[21]K. Saito and J. Kobayashi, Phys. Rev. B **45**, 10264 (1992).

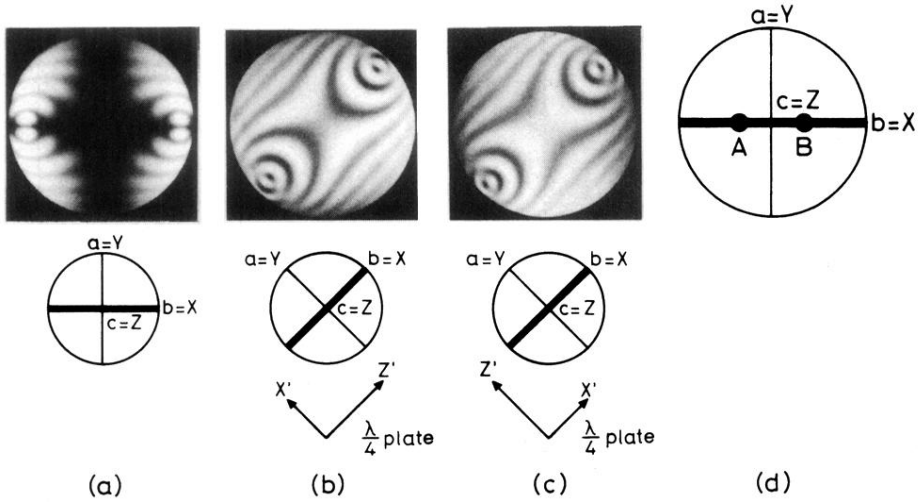

FIG. 2. Optical nature of Rb_2ZnCl_4 at room temperature (a) Conoscopic figure in the extinction position; (b), (c) conoscopic figures in the diagonal subtracting and adding conditions respectively produced by the insertion of the quarter-wavelength plates; and (d) stereographic representation of the optical nature.